Annu. Rev. Mater. Res. 2005. 35:99–126
doi: 10.1146/annurev.matsci.33.041002.094657

INFLUENCE OF INTERFACE ANISOTROPY ON GRAIN GROWTH AND COARSENING

Gregory S. Rohrer
Department of Materials Science and Engineering, Carnegie Mellon University, Pittsburgh, Pennsylvania 15213-3890; email: gr20@andrew.cmu.edu

Key Words grain boundaries, microstructure, polycrystal, crystal growth, interface energy

■ **Abstract** It has recently become possible to measure the anisotropic distribution of interfaces in polycrystals and composites. Because classical theories for grain growth and coarsening assume isotropic interface properties, they are incapable of explaining how these distributions arise. The purpose of this paper is to review the results of recent experiments, simulations, and theories that document the effects of anisotropy on the capillarity-driven evolution of granular systems. The results suggest that meaningful predictions of evolving microstructural characteristics can be made using models that incorporate the anisotropy of the interfacial energy and mobility.

INTRODUCTION

When a polycrystalline compact is heated at a temperature that is an appreciable fraction of its melting point, the sizes of the individual crystals change in such a way that the average grain size increases. This process is driven by a reduction in the total interfacial energy that occurs as the total interfacial area decreases. Because mass is conserved, some grains get smaller and disappear whereas others grow larger. In single-phase crystalline materials, where the grains are in intimate contact, this phenomenon is referred to as grain growth. When this process occurs in the midst of a distinct intervening phase that separates the crystals, it is usually referred to as coarsening. Because grain growth and coarsening are similar processes motivated by the same driving force, the two terms are frequently interchanged. In fact, without assigning a limiting value for the fractional volume of the intervening phase, a distinct classification may not be possible and, in many circumstances, the two processes may occur simultaneously. However, it should be recognized that distinct mechanisms are at work. In grain growth, the fundamental process is transferring an atom across a boundary from one grain to another. In coarsening, it is the dissolution of material from one crystal, its transport through the intervening phase, and precipitation onto another crystal that underpins the process.

1 Mar 2005 20:17 AR AR246-MR35-05.tex XMLPublish^{SM}(2004/02/24) P1: JRX
AR REVIEWS IN ADVANCE10.1146/annurev.matsci.33.041002.094657

There is an extensive literature on grain growth and coarsening that goes back more than 50 years and several reviews are available (1–3). One of the basic assumptions of the classical work is that the interface energies are isotropic. However, recent experiments and simulations have shown that anisotropy can have important consequences, particularly on the distribution of interface types. Furthermore, by classifying interfaces in a microstructure according to their crystallography, new metrics can be established to serve as a quantitative basis for understanding the relationship between the processing, structure, and properties of a material. In other words, accounting for anisotropy in growth processes not only has the potential to make more accurate predictions of polycrystalline structure, it also offers a way to characterize structural differences that have measurable influences on properties. Therefore, this review focuses on the influence of anisotropy on coarsening and grain growth and is constructed in the following way. The next section provides a summary of phenomenological observations of growth kinetics and size distributions. Classical theories and simulations of grain growth and coarsening are summarized in the third section. In the fourth section, the influence of anisotropic grain boundary and surface properties are discussed and in the fifth section, the impact of singular interfaces on growth is described. The final section identifies unanswered questions and likely trends for future research.

BRIEF ASSESSMENT OF EXPERIMENTALLY OBSERVED PHENOMENA

In a system of growing crystals, experimental observations consistently show that at a sufficiently high temperature, the average grain size increases with time until it approaches the sample size. For samples with anisotropic shapes, such as wires, films, or foils, the smallest dimension is the relevant size. The present discussion is limited to growth in three-dimensional systems where capillary forces dominate. Under these conditions, the time dependence of the average radius, $\langle r \rangle$, is

$$\langle r \rangle - \langle r_0 \rangle = (Kt)^n, \qquad 1.$$

where K is a positive constant, $\langle r_0 \rangle$ is the initial average radius, and n is a value less than or equal to $1/2$ (4–7). The upper limit of $1/2$ occurs for ideal conditions where the boundary velocity scales linearly with the capillary driving force. Smaller exponents are more frequently reported, and these results can be explained if there is a more complex driving force-velocity relationship determined by the presence of impurities (8, 9), pores, or second-phase precipitates (10). For the case of diffusion-limited coarsening, the exponent is $1/3$ (11). Although it has been convincingly demonstrated that in a sample of sufficient purity, grain growth at high temperature follows a kinetic law where $n = 1/2$, it should be recognized that this is an exceptional case and values of n less than $1/2$ are more typical (12).

Experimental observations also indicate that the rate of growth is inversely proportional to the size of the crystals (7):

1 Mar 2005 20:17 AR AR246-MR35-05.tex XMLPublish^{SM}(2004/02/24) P1: JRX
AR REVIEWS IN ADVANCE10.1146/annurev.matsci.33.041002.094657

$$\frac{d\langle r\rangle}{dt} = \frac{K}{\langle r\rangle}. \qquad 2.$$

Note that integration of Equation 2 gives Equation 1 with an exponent of 1/2. Because boundaries have been observed to move toward their centers of curvature, and the boundary velocity has been observed to be linearly dependent on the curvature, this phenomenon can be explained in terms of the capillary driving force, $\gamma\kappa$, where γ is the energy per unit area of the interface (assumed to be isotropic) and κ is the interface curvature (7, 13–15). Assuming uniform curvature, $\kappa = 2r^{-1}$, the boundary velocity decreases as $\langle r\rangle$ increases and, therefore, the rate of growth decreases with increasing average grain size.

In the late stages of grain growth and coarsening, it is believed that there is a characteristic distribution of crystal sizes that remains constant even as the average radius increases. In other words, the distribution at two different times is identical except for a change in the magnification. This is referred to statistical self-similarity or scaling. Whereas there is some experimental evidence for this assertion, it is difficult to demonstrate conclusively (16–18). As an example, grain size distributions (determined from true three-dimensional data) from four studies are compared in Figure 1*a* (19–22). The crystal size distributions are symmetric on a semilog plot and are most frequently reported to be lognormal:

$$f_L(\rho) = \frac{1}{(2\pi)^{1/2}}\frac{1}{\beta\rho}\exp[-(\ln\rho - \alpha)^2/2\beta^2], \qquad 3.$$

where $\rho = r/\langle r\rangle$, $\langle r\rangle$ is the average grain size, and α and β are fitting parameters. The lognormal distribution is shown in Figure 1*c*. Three reported distributions resulting from coarsening are illustrated in Figure 1*b* (18, 23, 24). Note that the first two distributions are similar, do not appear to be lognormal, and both result from the coarsening of a solid within a solid. The third, which is much broader and symmetric, results from coarsening in a liquid. It should also be noted that bimodal distributions are frequently observed in anisotropic systems; this phenomenon is usually referred to as abnormal growth. For example, during the coarsening of $BaTiO_3$, two distinct distributions of grains with average sizes in the ranges of 1 μm and 100 μm have been observed to coexist (25). The exact forms of these distributions and the kinetics of their evolution have not yet been studied in detail.

Topological characteristics in systems of coarsening particles vary widely depending on the volume fraction and characteristics of the intervening phase. For example, the coarsening phase may be fully faceted or bounded by curved interfaces, depending on the anisotropy of the interface energy. For grain growth in single-phase systems, on the other hand, the topology is determined by the simultaneous requirements that the grains fill all space while maintaining local equilibrium at the interfacial junctions (26). Therefore, grains are approximately polygonal volumes whose faces have slight curvatures. When the number of faces per grain is large enough, the interfacial equilibrium constraint forces the faces to be concave so that the grain expands at the expense of its neighbors.

1 Mar 2005 20:17 AR AR246-MR35-05.tex XMLPublish^{SM}(2004/02/24) P1: JRX
AR REVIEWS IN ADVANCE10.1146/annurev.matsci.33.041002.094657

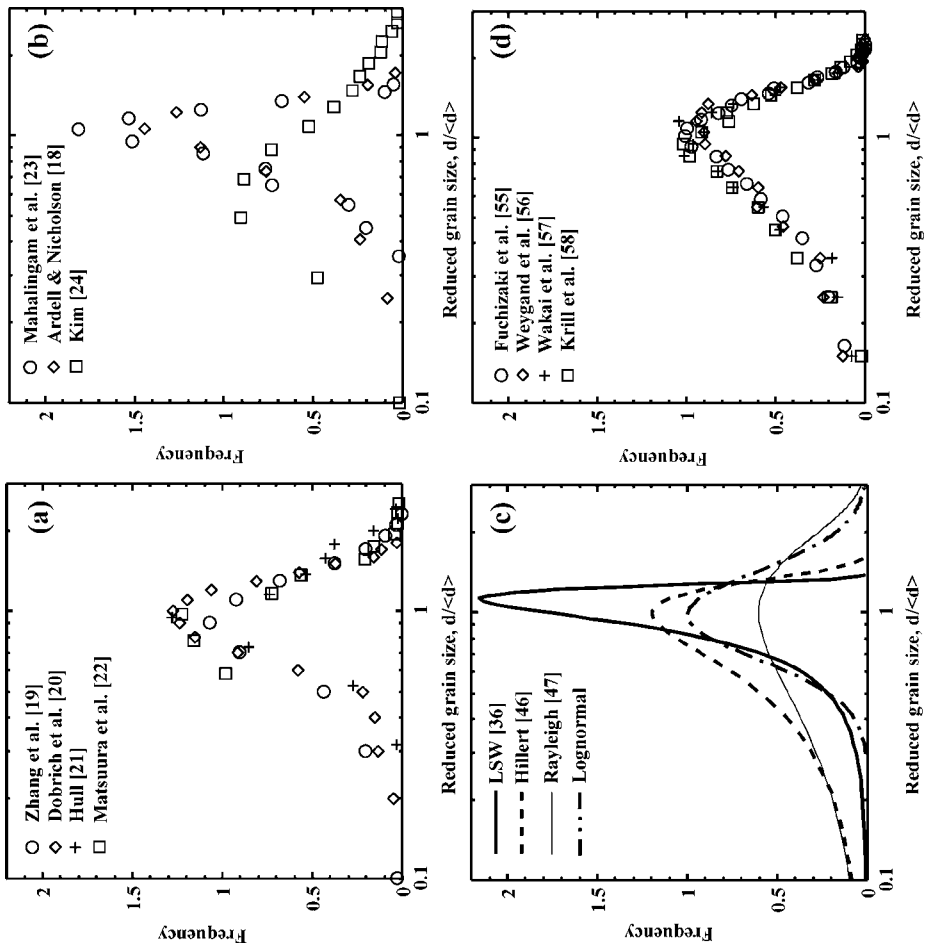

1 Mar 2005 20:17 AR AR246-MR35-05.tex XMLPublish^{SM}(2004/02/24) P1: JRX
AR REVIEWS IN ADVANCE10.1146/annurev.matsci.33.041002.094657

The implication is that larger, growing grains have more faces than smaller shrinking grains. This idea is supported by the observation that the average number of faces increases with the average crystal size, as illustrated in Figure 2. Measurements of the average number of faces per grain have yielded values between 12 and 14, whereas the average number of edges per faces is very close to 5 (19–22, 27).

Grain growth in nanostructured materials has been an active area of research during the past decade (28–30). A review of these experimental results suggests that for the most part, grain growth phenomena in the nanometer size range is much the same as it is in the micrometer size range: growth follows the kinetics of Equation 1 (29) and the crystal size distribution is roughly lognormal (31). Furthermore, the same things that slow growth in microcrystalline specimens, such as porosity and impurities, also retard the rates of grain growth in nanostructured materials. One difference is that the onset of growth usually occurs at lower temperatures. Furthermore, in at least some systems, anomalous kinetic behavior has been reported. For grain sizes below 150 nm, a linear growth exponent ($n = 1$) was observed in nanocrystalline Fe (32). Also, when growth data for microcrystalline Fe is extrapolated to the nanometer size range, a grain growth rate is predicted that is several orders of magnitude greater than what is actually observed (30). This and similar observations have led to speculation that alloying elements can stabilize nanocrystalline structures. Not only do they provide a drag force on the boundary, but adsorption can reduce the grain boundary energy, which leads to a diminished driving force for growth (33, 34).

In summary, experimental observations lead to the following conclusions about grain growth and coarsening. As a sample is annealed, the grain size increases in

←

Figure 1 Equal area histograms for reduced grain sizes from experiment (*a, b*), theory (*c*), and simulation (*d*). In each case, the histograms are normalized to the same area and plotted on the same domain to simplify the comparison. (*a*) Three- dimensional grain size measurements of a relatively large number of grains ($793 \leq N \leq 4966$). In each case, the linear dimension d is proportional to the cube root of the volume and normalized by the average of this value, $\langle d \rangle$. Zhang et al. (19), 793 Fe grains measured by serial sections. Döbrich et al. (20), 4966 grains of Al in Al-Sn by X-ray microtomography. Hull (21), 941 grains of brass, separated by mercury infiltration. Matsuura et al. (22), 1000 grains of 304 stainless steel separated by boundary corrosion. (*b*) Grain size distributions in coarsening systems, from observations of planar sections. Mahalingam et al. (23), Al 2.4w/o Li (Al_3Li in Al-Li) after 168 h at 200°C. Ardell & Nicholson (18), Ni 6.71%Al (Ni_3Al in Ni-Al) after 6 h at 775°C. Kim (24):WC in liquid Co. (*c*) Theoretical distributions. LSW (coarsening) (36), Hillert (grain growth or coarsening by surface attachment limited kinetics) (46), Louat (grain growth) (47), lognormal (Equation 3). (*d*) Grain size distribution predicted from three-dimensional simulation. Fuchizaki et al. (55), vertex dynamics model. Wegand et al. (56), vertex dynamics model. Wakai et al. (57), surface evolver. Krill et al. (58), phase field model.

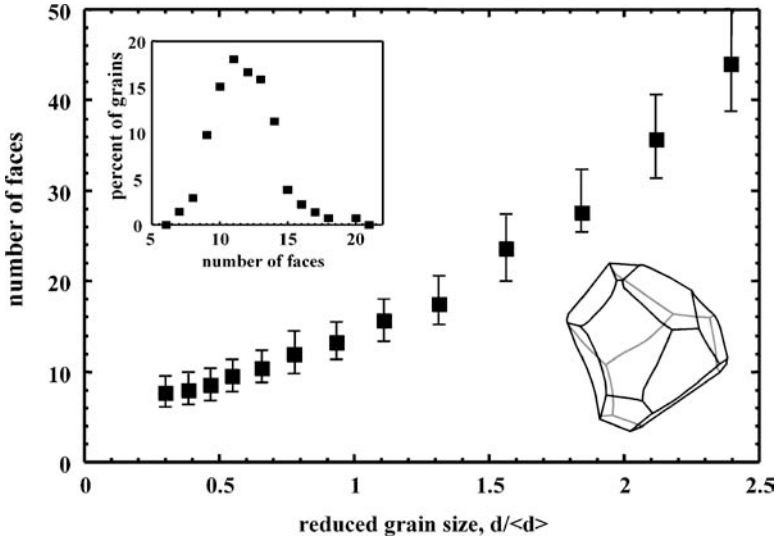

Figure 2 The number of grain faces as a function of reduced grain size (21). For each reduced grain size, the point represents the mean number of faces and the bars represent plus and minus one standard deviation. The upper inset shows the percentage of grains with different numbers of faces, and the lower inset shows a typical shape for a polygonal grain (27). Black lines show edges on the front of the grain and gray lines show edges on the back.

proportion to t^n, where n is less than or equal to $1/2$. Boundaries migrate toward their centers of curvature at a rate that is linearly proportional to the curvature. There is a characteristic distribution of crystal sizes that is constant with time in the late stages of growth, which is frequently described as lognormal. However, in numerous situations bimodal distributions are also observed. In cases where the growth is unimodal, the maximum grain size is usually two to three times the average. In dense polycrystals, the grains have on average 12 to 14 faces and 5 edges per face.

ASSESSMENT OF CLASSICAL THEORIES FOR GRAIN GROWTH AND COARSENING

In coarsening systems, crystals grow (or shrink) by the addition (or removal) of atoms that are transported to (or away from) the crystal by capillary-driven diffusion. In the classical theory, it is assumed that if the coarsening crystals are sufficiently far apart, then the intervening phase will serve as a reservoir at a fixed chemical potential of $\mu_\infty = 2\gamma/r^*$, where r^* is the radius of a crystal that neither shrinks nor grows in contact with this reservoir (35, 36). The driving force for each

1 Mar 2005 20:17 AR AR246-MR35-05.tex XMLPublish^{SM}(2004/02/24) P1: JRX
AR REVIEWS IN ADVANCE10.1146/annurev.matsci.33.041002.094657

crystal to grow or shrink is given by the free- energy difference between the atoms on the surface of a crystal with size r and the reservoir:

$$\Delta G = 2\gamma\Omega\left[\frac{1}{r^*} - \frac{1}{r}\right], \qquad 4.$$

where Ω is the molecular volume. The growth rate (dr/dt) of a crystal is proportional to this driving force and equal to either the rate of diffusion or the rate of the surface attachment/detachment process. When the evolution of the system is calculated, a kinetic law similar to Equation 1 is obtained where the exponent is $1/3$ for diffusion-limited kinetics and $1/2$ for surface attachment-limited kinetics. The time independent part of the distribution of crystal sizes resulting from diffusion-limited growth is (36)

$$f_{diff}(\rho) = \rho^2\left(\frac{3}{3+\rho}\right)^{7/3}\left(\frac{3/2}{3/2-\rho}\right)^{11/3}\exp\left[\frac{-\rho}{3/2-\rho}\right]. \qquad 5.$$

For the case of surface attachment-limited kinetics, the distribution is (36)

$$f_{salk}(\rho) = \rho\left(\frac{2}{2-\rho}\right)^5\exp[-3\rho/(2-\rho)]. \qquad 6.$$

Both distributions are plotted in Figure 1*c*. The classical coarsening theory was originally formulated under the assumption that the coarsening crystals were so far apart that their diffusion fields do not overlap. This occurs as the crystal volume fraction approaches zero. Real systems have finite volume fractions of the coarsening phase and several modifications have been made to the original theory to account for this (36–39). The corrections do not influence the growth exponent, but they do lead to broader and more symmetric particle size distributions that are a closer approximation to the experiment.

The elementary process during grain growth is the change in the position of a grain boundary as volume is transferred from one grain to another. The theories to account for this process fall into two broad classes: those rooted in topology and those rooted in stochastic behavior. The fundamental premise of the topological models is the von Neumann-Mullins (40) rule for growth in two-dimensional systems. As long as the grain boundary energies are isotropic, then the dihedral angles where three grain boundaries meet must all be 120°. Therefore, grains with more than six sides have concave boundaries and will grow and grains with fewer than six sides will have convex boundaries and shrink. This leads to the so-called N-6 rule for grain growth in two dimensions:

$$\frac{dA}{dt} = M\gamma\frac{\pi}{3}(N-6), \qquad 7.$$

where M is the boundary mobility, A is the grain area, and N is the number of sides. Theorists have sought a similar rule for three-dimensional growth (41, 42, 45). Assuming that the number of faces in three dimensions is analogous to the

1 Mar 2005 20:17 AR AR246-MR35-05.tex XMLPublish^{SM}(2004/02/24) P1: JRX
AR REVIEWS IN ADVANCE10.1146/annurev.matsci.33.041002.094657

number of sides in two dimensions, expressions have been produced that yield a zero growth rate when the number of faces is between 13 and 14. However, the complication is that there is no three-dimensional polyhedron that simultaneously fills space and satisfies the interfacial equilibrium constraints at the junctions. The assumed existence of such a critical polyhedron, and the correlation between size and number of faces (see Figure 2), led Hillert (46) to propose that there is a characteristic grain size above which all grains grow and below which all grains shrink. On this basis, he proposed a driving force in analogy to Equation 4 and developed a model that yields a parabolic growth law and the crystal size distribution, as illustrated in Figure 1*c*:

$$f_H(\rho) = (2e)^3 \frac{3\rho}{(2-\rho)^5} \exp[-6/(2-\rho)]. \quad 8.$$

This distribution is identical (except for a scale factor) to that resulting from coarsening with surface attachment-limited kinetics (see Equation 6). It is less symmetric than the observed grain sized distributions in Figure 1*a* and predicts a much smaller maximum grain size.

Stochastic theories of grain growth assume grain sizes change randomly (47), i.e., crystals execute a random walk through the space of sizes. More elaborate theories combine a random term with a curvature-driven term that biases the random walk so that larger grains are more likely to grow and smaller grains are more likely to shrink (48–51). Depending on the exact formulation of the model, growth exponents varying from 1/4 to 1/2 arise, and the distribution of crystal sizes is usually given by the Rayleigh distribution, shown in Figure 1*c*.

$$f_R(\rho) = \frac{\alpha\rho}{\beta} \exp[-\rho^2/4\beta]. \quad 9.$$

Although it is plausible that the motions of all boundaries, when averaged over a long time, behave randomly, these models are counterintuitive because experimental observations illustrate that individual boundaries move in a predictable way toward their centers of curvature. Furthermore, the purely stochastic model has been criticized because it does not conserve volume (49, 50, 51a), and it has been argued that in combined models, random fluctuations in size are incompatible with the condition for continuity in self-similar growth (52).

It must be noted that observed crystal size distributions do not (in general) match well with the theoretical predictions (see Figure 1). However, it has been pointed out that the Hillert distribution is predicated on the basis of an assumed linear relationship between the grain size and the average number of faces. If this distribution has modest nonlinearities (as appears to be the case in Figure 2), the crystal size distribution has been shown to be quite different (53).

Three-dimensional grain growth simulations are expected to produce a more realistic account of the process, and numerous results have been published in recent years. Calculations based on the Monte Carlo Potts model (54), vertex tracking (55, 56), boundary tracking (57), phase field (58), and gradient-weighted moving

1 Mar 2005 20:17 AR AR246-MR35-05.tex XMLPublish^{SM}(2004/02/24) P1: JRX
AR REVIEWS IN ADVANCE10.1146/annurev.matsci.33.041002.094657

finite elements (59) have been used to simulate the structure and evolution of grain boundary networks in three-dimensional systems. Until very recently, the simulations have used only isotropic grain boundary properties. The grain size distributions resulting from these models are illustrated in Figure 1*d*. Note that whereas the distributions are all similar, they are also distinct from the experimental distributions. All exhibit the shape characteristic of the theoretical distributions (Figure 1*c*).

For the theories described above, it is assumed that boundary motion is the limiting step in growth. More recently, however, several theories have emerged for growth limited by other factors. One is the vacancy drag model (60–62). Grain boundaries have an excess volume per area on the order of 0.02 nm. As grain growth occurs and interfacial area is eliminated, the excess volume must also be eliminated, presumably in the form of vacancies. If the diffusion of vacancies through the bulk is the rate limiting step, then linear ($n = 1$) growth kinetics are expected. The possibility that vacancy elimination is rate limiting is expected only at nanometer scale grain sizes and might explain the nonclassical kinetics observed in nanocrystalline Fe (32). A second possibility is that the motion of triple junctions becomes rate limiting (60). The usual assumption is that in equilibrium, the resolved force on the moving triple junction is zero. However, if the triple junction has a low intrinsic mobility, or if its motion is limited by impurities, then there is a net retarding force on the moving junction that will make the dihedral angles differ from the equilibrium value. Because of these changes in the dihedral angles, there is no unique topological class that divides growing grains from shrinking grains in two dimensions. This influence of the triple junctions will be greatest at the smallest grain sizes (2, 63). It has also been shown that at very small grain sizes, the random characteristics of atomic motion may influence grain growth (64). For the smallest grain sizes, stochastic atomic jumps determine the kinetics of grain growth and an exponent of $1/4$ is predicted, with a transition of $1/2$ by the time the grains reach an average size of 20 nm.

INTERFACE ANISOTROPY

One of the assumptions underpinning all of the theories described in the previous section is that the interface properties are isotropic. Whereas the surface energies of metals near their melting points might be reasonably approximated as being isotropic, it is well known that the surface energies of many ceramics (65, 66) and the grain boundary energies and mobilities of almost all materials vary with the character of the interface (67, 68). The grain boundary character distribution, $\lambda(\Delta g, \mathbf{n})$, can be defined as the relative areas of distinguishable grain boundaries characterized by their lattice misorientation (Δg) and boundary plane orientation ($\mathbf{n}$). Because the misorientation depends on three independent parameters, and the boundary inclination on two, the domain of grain boundary types is five-dimensional, and the number of distinguishable grain boundaries is large (69).

1 Mar 2005 20:17 AR AR246-MR35-05.tex XMLPublish^{SM}(2004/02/24) P1: JRX
AR REVIEWS IN ADVANCE10.1146/annurev.matsci.33.041002.094657

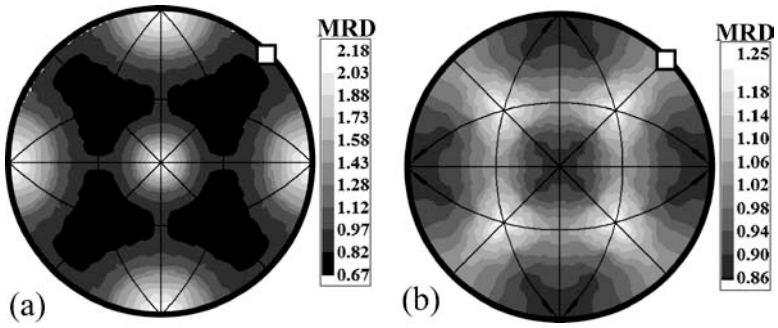

Figure 3 The distribution of grain boundary planes averaged over all misorientations for (*a*) MgO (70) and (*b*) Al (74). In the case of MgO, {100} planes are preferred; in the case of Al, the preference is for {111} planes. The data are shown in stereographic projection along [001], which is in the center of each projection. The [110] direction is marked with a square in each projection. The units are multiples of a random distribution (MRD).

The grain boundary character distribution can be thought of as a metric by which the structure of a polycrystal can be quantified.

Recent measurements of the grain boundary character distribution in a diverse range of ceramics and metals, including MgO (70), $SrTiO_3$ (71), TiO_2 (72), $MgAl_2O_4$ (73), Al (74), Fe-1%Si (75), have led to three important conclusions. (*a*) The first is that the distribution of grain boundary planes is anisotropic (see Figure 3). (*b*) Second, the preferred habit planes for grains within polycrystals correspond to the same low-energy, low-index planes that dominate the external growth forms and equilibrium shapes of isolated crystals of the same phase (72). This finding amounts to a paradigm shift in our understanding of grain boundaries, which has been dominated for decades by consideration of crystal lattice orientation relationships instead of the grain surface relationships that have been found to be more influential. Furthermore, a correlation has been identified between the sum of the surface free energies that make up the boundaries and the grain boundary energy, $\gamma(\Delta g, \mathbf{n})$ (71, 76). This finding, derived from observations in a wide range of materials, provides an extremely useful simplifying principle: Knowledge of the surface energy anisotropy, which depends on only two parameters, is sufficient for predicting the grain boundary energy. (*c*) The third important finding is that the grain boundary character distribution is correlated to grain boundary energies, $\gamma(\Delta g, \mathbf{n})$ (76, 77). This is illustrated in Figure 4, which shows that low-energy boundaries occur more frequently in the distribution than high-energy boundaries.

Whereas it is now clear that anisotropic boundary properties influence the grain boundary character distribution, it is not yet clear how the distribution forms during growth. One particularly striking example of the importance of anisotropy to growth was described in a recent attempt to deterministically predict the evolution of a specific grain boundary network (78). The grain boundary network structure of

1 Mar 2005 20:17 AR AR246-MR35-05.tex XMLPublish[SM](2004/02/24) P1: JRX
AR REVIEWS IN ADVANCE10.1146/annurev.matsci.33.041002.094657

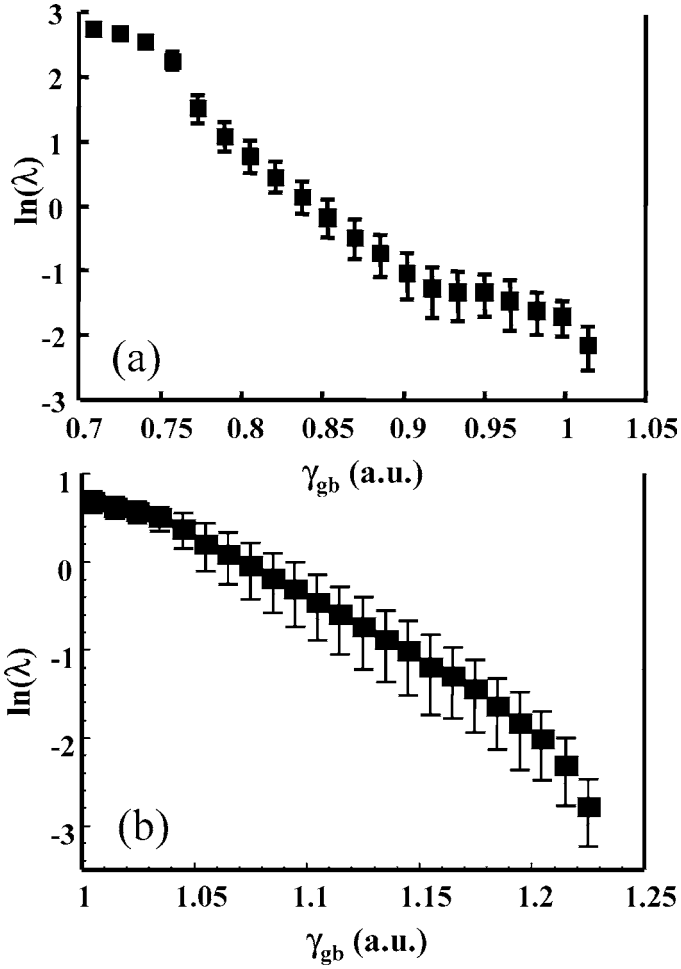

Figure 4 The logarithm of the grain boundary population (λ) as a function of the grain boundary energy (γ_{gb}). The mean is represented by the point; the bars indicate one standard deviation. Panel (*a*) is based on experimental observation (76) and panel (*b*) results from three-dimensional grain growth simulations with isotropic properties (77).

a columnar Al sample was mapped using orientation imaging microscopy over an area consisting of more than 5000 grains. The sample was then annealed to allow the microstructure to evolve, and the orientation mapping was repeated. The initial grain structure was then used as the starting configuration for a curvature-driven grain growth simulation. Simulations were performed assuming isotropic grain boundary properties in one case and anisotropic properties in other cases. The simulations based on measured anisotropic properties reproduced the observed

1 Mar 2005 20:17 AR AR246-MR35-05.tex XMLPublish^{SM}(2004/02/24) P1: JRX
AR REVIEWS IN ADVANCE10.1146/annurev.matsci.33.041002.094657

microstructural evolution much better than the isotropic properties. The implications of this experiment are clear: To realistically predict how a microstructure will evolve, it is necessary to include the correct properties of individual boundaries.

Although this example demonstrates the importance of anisotropy in influencing the movement of specific boundaries, it is perhaps more important to understand the effect of anisotropy on statistically averaged properties of the microstructure that are more accessible to experiment. Mullins (79) showed that as long as the crystal size distribution maintains statistical self-similarity during growth and the interface energy is differentiable at all orientations, then the anisotropy of the interface energy does not influence the normal kinetic laws for coarsening and grain growth. Furthermore, a one-dimensional capillary grain growth model demonstrated that for anisotropic boundary properties, a statistically similar particle size distribution is obtained and the distribution is different from that which results from uniform boundary properties (80). Two-dimensional coarsening models have also indicated that the crystal size distribution is influenced by interface energy anisotropy (81, 82). These results reproduced Mullins' predictions that anisotropy does not affect growth kinetics, but it does weakly influence the distribution of crystal sizes. Recent experimental studies of shape evolution during coarsening have shown a trend toward a greater population of low-index surfaces as growth proceeds. For $SrTiO_3$ coarsening in a TiO_2-rich eutectic liquid and PMN/PT coarsening in a PbO-rich liquid, it was observed that crystals with approximately isotropic initial shapes evolve to more polygonal forms bounded by low-energy surfaces (83, 84).

Experimentally, it is not usually possible to separate the comparative influence of the interface energy and mobility on the development of the interface character. However, simulations are capable to doing this. A number of two-dimensional simulations of capillary-driven grain growth indicate that the grain boundary energy plays a pivotal role in determining the grain boundary character distribution. Holm et al. (85) showed that the steady-state misorientation distributions in anisotropic systems vary with the assumed boundary energy anisotropy, which depend only on the lattice misorientation. The anisotropy of the mobility was not an important factor in this simulation. Grain boundaries with low energy were enhanced in the population when the data were weighted by length. However, the number densities of the boundaries were not changed by the energy anisotropy. In this case, it was concluded that the lower energy boundaries lengthened to achieve local equilibrium configurations at the grain boundary triple junctions. Simulations by Upmanyu et al. (86) used more complex forms of the energy and mobility anisotropy derived from molecular dynamics simulations, but with a simplified (one angular parameter) model for the grain misorientation. The results were similar to those of Holm et al. (85): A steady-state distribution of misorientations developed that was inversely related to the assumed grain boundary energy and relatively unaffected by the grain boundary mobility.

In both of the simulations described above, the energy of the grain boundary depended on only the lattice misorientation and not on the orientation of the interface. Kinderlehrer et al. (87) used a two-dimensional simulation to examine

1 Mar 2005 20:17 AR AR246-MR35-05.tex XMLPublish[SM](2004/02/24) P1: JRX
AR REVIEWS IN ADVANCE10.1146/annurev.matsci.33.041002.094657

the effects of both lattice misorientation and boundary plane inclination on the distribution. When the grain boundary energy depends on only the lattice misorientation, the population and energy are related by the Boltzman distribution. This is reminiscent of the results in Figure 4, which shows that the logarithm of the population decreases linearly with grain boundary energy. When the grain boundary energy also depends on the orientation of the interface plane, the distribution appears to depend on both the energies and the gradients in the energies. Note that the orientation dependence of the energy and population that results from the model (Figure 5*a*) is similar to the trends in the observed values (Figure 5*b*). This

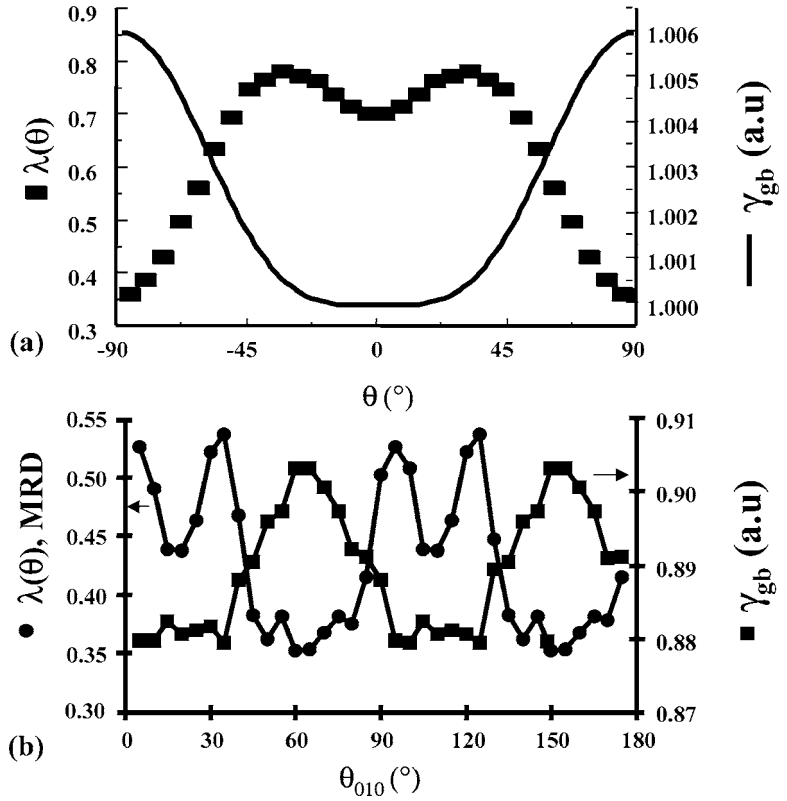

Figure 5 (*a*) Comparison of a simulated grain boundary character distribution and the assumed energy anisotropy as a function of the boundary normal (87). (*b*) Comparison of measured grain boundary energies (squares) and the observed population distribution (*circles*) for Σ5 tilt boundaries in MgO (76). The quantities are plotted in 5° intervals as a function of θ_{010}, the angle between [010] and the grain boundary normal. Note that in both cases, the population reaches a maximum at the positions where the gradient changes from being steeply negative to approximately zero.

1 Mar 2005 20:17 AR AR246-MR35-05.tex XMLPublish^{SM}(2004/02/24) P1: JRX
AR REVIEWS IN ADVANCE10.1146/annurev.matsci.33.041002.094657

sensitivity to the gradient of the energy is likely the source of the distribution in the populations at each energy value in Figure 4. As in the other simulations, it was found that the mobility has a subordinate effect on the distribution.

During microstructural evolution, the distribution changes most significantly when a boundary is annihilated in a neighbor switching or grain collapse event. It is known that as a grain loses sides, it is the shortest boundary that is lost first. If length is inversely correlated to energy, as suggested by Holm et al. (85), then we see that higher-energy boundaries are preferentially annihilated, and low-energy boundaries will form a greater portion of the population, as illustrated in Figures 4 and 5. Simultaneously, there are new boundaries being created, but as long as there is little texture, these should simply add a random component to the population. The abrupt creation and annihilation of boundaries means that triple junctions must adjust to accommodate these changes. If the energy depends on only misorientation, then the boundary plane can rotate without changing energy. However, when boundary plane anisotropy is included, these adjustments in position will occur in proportion to the torque (the differential of energy with respect to orientation) on the plane; this explains why the population is also affected by the gradients in the energy (see Figure 5).

The reorientation events that change the boundary character without changing the lattice misorientation are most likely to occur at the triple junctions, where boundaries are free to rotate to achieve a balance of the interfacial tensions and torques. When a simulation was run with anisotropic grain boundary energies, but also with the boundary condition that all triple-junction dihedral angles be $2\pi/3$ (the condition for isotropy), the grain boundary character distribution remained isotropic. From this result, it can be concluded that it is local adjustments at the triple junctions that lead to the anisotropy in the steady-state grain boundary character distribution.

The first simulations of anisotropic grain growth in three dimensions, using boundary properties that depend on all five crystallographic parameters and a statistically significant number of grain boundaries, have recently been completed. Using Grain3D, Gruber et al. (77) measured the evolution of the grain boundary character distribution as a function of time. In the initial state, there were more than 41,000 grains, and the grain boundary character distribution was completely isotropic. During the course of the simulated growth, approximately 30% of the total interfacial area and 75% of all the grains were eliminated. However, as illustrated in Figure 6, the distribution of interface planes reaches a steady state relatively quickly. In Figure 7, the distribution of grain boundary planes that develops from the initially random distribution, averaged over all misorientations, is compared with the assumed energy anisotropy. The approximate inverse relationship between energy and population evident in Figure 4 and 5 is also obvious here. Note that the distribution in Figure 7*a* is a statistically self-similar steady state that remains constant even as the network continues to evolve by normal growth. This is analogous to the self-similar grain size distributions predicted by the classical growth models.

Whereas mobility anisotropies do not appear to affect the grain boundary character distribution in materials with random orientation distributions, recent

1 Mar 2005 20:17 AR AR246-MR35-05.tex XMLPublish[SM](2004/02/24) P1: JRX
AR REVIEWS IN ADVANCE10.1146/annurev.matsci.33.041002.094657

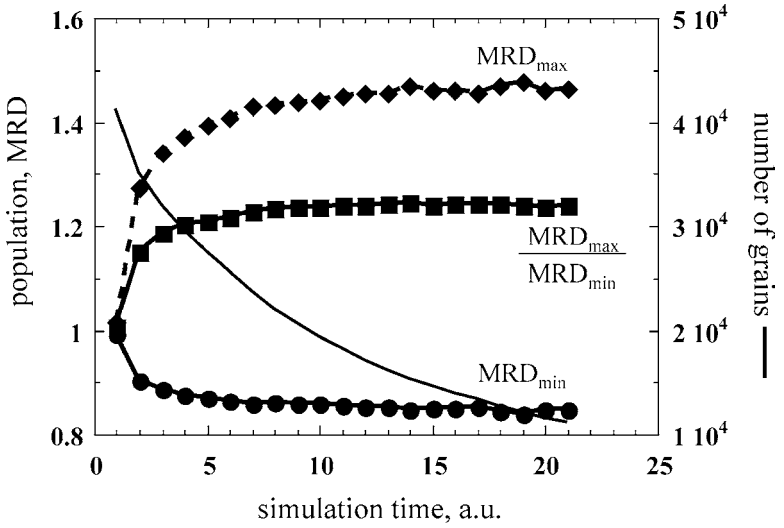

Figure 6 Simulated changes in the grain boundary character distribution with time (77). In the initial distribution, all boundaries occurred with the same frequency. As the number of grains is reduced by grain growth, the maxima and minima of the distribution (see Figure 7) reach steady-state values.

three-dimensional Monte-Carlo simulations of grain growth in a deformed and textured matrix suggest that mobility anisotropy can influence the development of grain orientation texture and, therefore, the grain boundary character distribution (88). In the initial condition, the model polycrystal was assigned a conventional rolling texture normally associated with an fcc metal deformed in plane strain; it

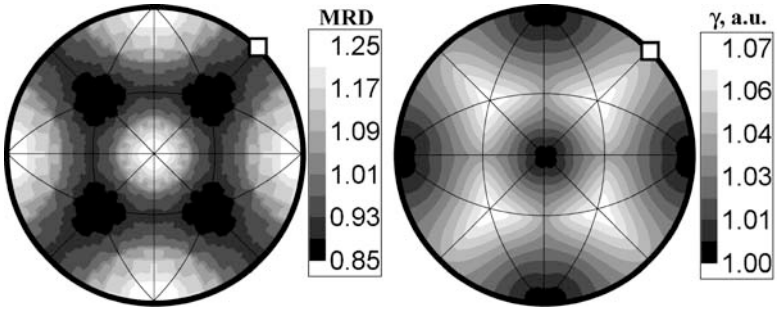

Figure 7 (*a*) The simulated distribution of grain boundary planes averaged over all misorientations, after the distribution has reached a steady state (time = 10 in Figure 6) (77). (*b*) The assumed variation of the grain boundary energy as a function of grain boundary plane orientation, provided as input for the simulation. The reference frames for the projections are the same as in Figure 3.

1 Mar 2005 20:17 AR AR246-MR35-05.tex XMLPublish^{SM}(2004/02/24) P1: JRX
AR REVIEWS IN ADVANCE10.1146/annurev.matsci.33.041002.094657

was also "seeded" with a small volume fraction of grains with the cube texture, $\{001\}\langle 100\rangle$. Mobility anisotropies with peaks for boundaries with a 40° misorientation about [111] were assigned to reflect experimentally measured anisotropies (89). The simulations showed that the greater the mobility of the $40^\circ/\langle 111\rangle$ boundary, the greater the volume fraction of material with cube texture in the resulting microstructure. From this it was concluded that the presence of a peak in the mobility centered on the 40° about $\langle 111\rangle$ boundary type leads to the growth of the cube texture component.

To summarize, the steady-state kinetics of growth processes are not expected to be influenced by interface anisotropy; the grain size distribution is weakly influenced by anisotropy, and the interface character distribution is significantly influenced. Experiments and simulations suggest that steady-state interface character distributions are obtained during growth and, for the case of grain boundaries, the distribution is related to both the energy and the gradients of the energy with respect to the interface orientation. Boundary mobilities have little influence on the interface character distribution in randomly oriented systems but apparently do influence the development of the grain boundary character distribution in systems that have some texture in the initial state. In comparison with the distribution of grain sizes, the interface character distribution is a superior metric for differentiating microstructures and is expected, therefore, to provide a clearer link to materials properties.

INFLUENCE OF SINGULAR INTERFACES ON GROWTH PHENOMENA

Classical grain growth and coarsening theories assume isotropic interface energies and that all interfaces move by the same mechanism. However, it has been recognized for many decades that the mechanisms by which interfaces move depend to some extent on the interface structure. On atomically rough surfaces (assumed in classical theories), atoms can be added or removed from kink sites, and the rate of growth is generally limited by the rate at which reactants reach (or attach to) the surface. Singular or nonrough surfaces, which correspond to cusps in the plot of the surface energy as a function of orientation, advance or retreat via the lateral motion of steps that add or subtract atomic layers (90). If the singular surface has no steps or step sources (such as screw dislocations or twin plane reentrant edges), its motion is then limited by the rate of two-dimensional nucleation. One characteristic of materials exhibiting abnormal growth phenomena is that their microstructures contain a mixture of curved (rough) and flat (singular) interfaces. Therefore, it is reasonable to assume that the rates at which these interfaces move are controlled by different mechanisms. The important point here is that if these two mechanisms occur at very different rates, then it is possible to imagine how bimodal grain size distributions arise in some materials. This point has been the subject of numerous recent studies and is described further in the remainder of this section.

1 Mar 2005 20:17 AR AR246-MR35-05.tex XMLPublish[SM](2004/02/24) P1: JRX
AR REVIEWS IN ADVANCE10.1146/annurev.matsci.33.041002.094657

We begin with a consideration of how nucleation on a singular interface affects the coarsening of crystals bounded by singular interfaces. To simplify the situation, we begin with a collection of cube-shaped crystals with surface energy γ and a distribution of edge lengths, L. The crystals are dispersed in an intervening phase and the chemical potential of the material dissolved in that phase is $\mu_\infty = 2\gamma/r^*$. Therefore, there is a crystal size $L^* = 2r^*$ that is in equilibrium with the intervening phase. We can now consider the energy involved in transferring material from the intervening phase to the surface of the crystal. To do this, we place a square nucleus of area s^2 and height a on the flat facet, where the chemical potential is zero. The energy for this transfer is

$$\varepsilon(s) = 4as\gamma - as^2\frac{2\gamma}{r^*} \qquad 10.$$

for $0 \leq s \leq L$. In Equation 10, the first term on the right hand side is the energy of the perimeter of the nucleus and the second term is the change in the free energy on moving a volume of material (as^2) from the intervening phase to the flat surface. Equation 10 shows that the energy change on adding a complete layer ($s = L$) to a crystal with size $L = 2r^*$ is zero, as expected; however, before the layer is completed, the crystal must pass through a relatively higher energy state that contains a partial layer. By differentiation, we see that the maximum occurs at $s = r^*$ and that the barrier to addition is $\varepsilon_+ = 2a\gamma r^*$, where $0 < r^* < L$. It is interesting to note that the barrier for adding layers is independent of the size of the growing crystal and mainly governed by r^*, which is a measure of the average size of crystals in the system.

To remove material from the crystal and dissolve it in the intervening phase, the change in energy is

$$\varepsilon(s) = 4as\gamma - 4aL\gamma + (aL^2 - as^2)\frac{2\gamma}{r^*}. \qquad 11.$$

In the expression above, the first two terms on the right hand side represent the energy difference between a complete layer and a partial layer; this is ≤ 0 for all valid values of s. The final term on the right hand side is the energy increase associated with moving a volume of material from the flat surface to the reservoir. The maximum of Equation 11 is at $s = r^*$ and the barrier to removing a layer, ε_-, is

$$\varepsilon_- = 2a\gamma\left[r^* + L\left(\frac{L}{r^*} - 2\right)\right], \qquad 12.$$

where r^* is between $L/2$ and L. Note that for a crystal of size $L = 2r^*$, $\varepsilon_+ = \varepsilon_- = 2a\gamma r^*$, as expected for the equilibrium case. For smaller crystals, the barrier decreases (see Figure 8) and vanishes completely for crystals with $r^* = L$. More generalized forms of these barriers have been derived previously, but the simplified forms given above are acceptable for the present purposes and do not lead to different conclusions (91).

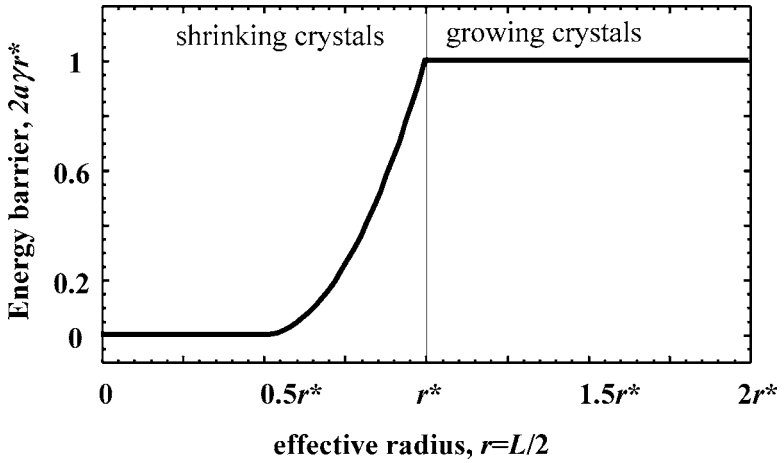

Figure 8 Plot of the nucleation energy barrier for crystals of different sizes in contact with a reservoir with a chemical potential $2\gamma/r^*$.

It is first important to compare the size of these barriers with the available thermal energy and the potential energy supplied by capillarity. The most important barrier is the one for the growth of crystals with sizes $L \geq 2r^*$ (this is the largest barrier). Even though small crystals can shrink without a barrier, the constraint of mass conservation will restrict their ability to do so if the barrier for growth is too large. In a typical situation that might be realized in the laboratory, we can take a to be 2×10^{-10} m, γ to be 1 J/m^2, and r^* to be 500 nm. To a first approximation, the choice of r^* is set to the average size of the crystals in the coarsening compact, and 500 nm is taken as a lower limit for most practical cases; this leads to a barrier to growth of 2×10^{-16} J. The relevant energies for comparison are the energy change resulting from capillarity-driven growth (taken to be $2\gamma a^3/r^* = 3 \times 10^{-23}$ J) and the available thermal energy ($kT = 2 \times 10^{-20}$ J at 1500°C). Although these calculations are admittedly approximate, several things are clear. First, because the barrier energy for growth on micron-sized crystals is more than 10^6 times the capillary driving force, we can be certain that capillarity cannot drive nucleation. In fact, for all cases where the grain size is larger than a few nm, if nucleation occurs, it must be driven by thermal fluctuations. The second point is that even thermal fluctuations are unlikely to drive nucleation on large crystals. According to the estimates above, the nucleation energy barrier is 10^4 kT. It has been estimated that barriers greater than 40 kT are not overcome in reasonable time periods (92). It should be noted that the step edge energy is usually thought to be a fraction of the surface energy, so the barrier height given above is probably overestimated. However, the nucleus perimeter energy would have to be reduced by a factor of 100, to 0.01 J/m^2 before the barrier would be reduced to 40 kT. Since this is considered unlikely, the size of the barrier energy and the extremely small driving force implies

1 Mar 2005 20:17 AR AR246-MR35-05.tex XMLPublish^{SM}(2004/02/24) P1: JRX
AR REVIEWS IN ADVANCE10.1146/annurev.matsci.33.041002.094657

that singular interfaces without defects should never advance outward during coarsening (93).

For comparison, we should also consider the conditions under which two-dimensional nucleation can be expected to occur and has been observed experimentally. The theory for two-dimensional nucleation shows that the nucleation rate decreases exponentially as the ratio of the driving force to the available thermal energy decreases and as the ratio of the perimeter energy to the available thermal energy increases (94). In accordance with the theory, two-dimensional nucleation has been observed in cases where driving forces comparable to the thermal energy are provided by supersaturated liquids or vapors, or by cooling a melt below the crystallization temperature. For example, growth by two-dimensional nucleation has been reported during the solidification of liquid Ga, where the driving force is supplied by the latent heat of crystallization, which is greater than the available thermal energy (95, 96). In this case, it is also relevant to note that solid-liquid interface energy is very low (in the range of 0.04 to 0.07 J/m^2) and that the nucleus perimeter energy was determined to be in the range of 0.01 to 0.02 J/m^2. So, in addition to a high driving force, the nucleation energy barrier is significantly reduced by the low interfacial energy. The transition from dislocation controlled growth to two-dimensional nucleation controlled growth has been observed during the vapor deposition of NaCl (97). It was reported that the transition to two-dimensional nucleation occurs when the driving force exceeds 0.09 eV at 347°C. At this point, the driving force is approximately twice the thermal energy. In summary, two-dimensional nucleation has been observed in the past when the driving force is relatively large and comparable to the available thermal energy. In contrast, the capillary driving forces that arise during the coarsening of micron-sized crystals are only a small fraction of the thermal energy.

Several authors have argued that the growth mechanisms associated with singular interfaces can be used to explain abnormal growth phenomena. Through the analysis of microstructural data from many different systems, Yoon and coworkers (98) have noted that abnormal growth phenomena occur when singular interfaces are present in the system and that systems with fully rough interfaces grow normally. Their explanation is that abnormal growth is attributed to the step migration growth mechanisms of singular surfaces. Two different mechanisms have been invoked. The first, articulated in Reference 99 and citations therein, is that some grains can become large enough that the capillary driving force is higher than the critical value for the onset of nucleation, and this leads to abnormal growth. However, on the basis of the numerical estimates made in the paragraph above, this explanation is not viable. One reason is that under typical experimental conditions, the energies associated with thermal fluctuations are much larger than the capillarity driving force so that nucleation will be driven by thermal fluctuations or not at all. Another reason that the explanation is not viable is that all growing crystals are subject to the same barrier ($\varepsilon_+ = 2a\gamma r^*$) so that the size of the growing crystal is simply not a relevant factor; if two-dimensional nucleation by thermal fluctuations is possible on one growing crystal then it will occur on all

1 Mar 2005 20:17 AR AR246-MR35-05.tex XMLPublish^{SM}(2004/02/24) P1: JRX
AR REVIEWS IN ADVANCE10.1146/annurev.matsci.33.041002.094657

growing crystals exposed to the same mean field chemical potential. The second possible mechanism is that step-producing structural defects, expected to occur in a subset of the crystals, allow the defective population to grow without a barrier and thus the average size of this subset becomes much larger than the more perfect crystals. It seems clear that having two distinct populations growing at very different rates is a plausible explanation for abnormal growth. However, a subset of large crystals growing by capillarity driven two-dimensional nucleation is not plausible.

The defect-controlled coarsening mechanism has been studied in detail and numerical simulations based on this model have demonstrated its feasibility (91). In the case where the growth of mixed populations is modeled (some crystals are limited by the barrier and others are assumed to have defects), bimodal populations are observed where the defect-containing subset of crystals grows much faster than the others, as illustrated in Figure 9. Note that because the smallest crystals in the slow population are able to shrink without a barrier (see Equation 12), they sustain the growth of the minority population of defective crystals.

The nucleation-limited coarsening model makes a number of predictions that can be compared with those of experiments. The first is that abnormal growth should be transient. In other words, at some point the defective (fast growing) grains have completely consumed the ideal (slow growing) population; because none of the remaining population has an advantage, growth should then proceed normally. The second is that during the period of bimodal growth, the number density of the large grains should remain constant, whereas the number of small grains should decrease. Although detailed measurements of the evolution of the grain size distribution are not yet available, some reports in the literature are consistent with this model (25).

The dislocation density in large $SrTiO_3$ seed crystals has been correlated with the rate at which they grow into a polycrystalline compact (100). Although there were only two observations, the seed with a higher dislocation density had a higher growth rate. Orientation imaging microscopy data suggest that all abnormal grains in PMN/PT have a twin (a boundary with a 60° rotation about ⟨111⟩). Twins are not found in the smaller matrix grains (101, 102), and these observations have been used to suggest that the reentrant twin plane edge provides a nucleation site with a greatly reduced barrier that allows the twinned crystals to grow much faster than the untwinned crystals. However, it should be noted that by observing only the final state, it is not possible to determine if the twin caused the grain to become large or if twins arise naturally in all grains when they become large. It can be reasoned that any grain that grows large enough will have encountered grains of many other orientations. In a random orientation distribution, approximately 1 in 50 misorientations will be close to the twin relationship (103). Thus, if a grain grows so that it has encountered many more than 50 differently oriented grains, it is likely that a twin will be formed, and this may be the reason that all large grains have twins. The independence of twinning and high growth rates was demonstrated in a recent paper where it was shown that there is no measurable difference in the growth rates of twinned and untwinned seeds (104). Since these

1 Mar 2005 20:17 AR AR246-MR35-05.tex XMLPublish^{SM}(2004/02/24) P1: JRX
AR REVIEWS IN ADVANCE10.1146/annurev.matsci.33.041002.094657

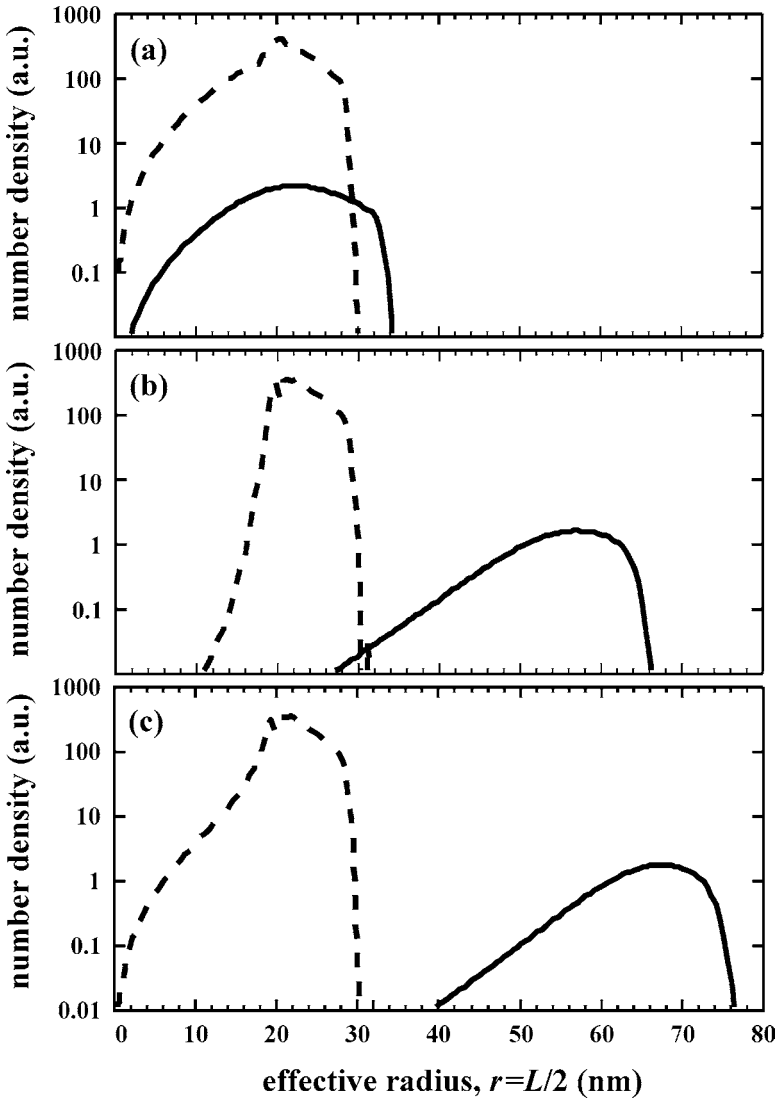

Figure 9 Simulated crystal size distribution for the defect-free crystals (*dashed line*) and the crystals with a persistent step source (*solid line*) coarsening in the same system: (*a*) after 1 arbitrary unit of time, (*b*) after 8, (*c*) after 11. The crystals with the step source grow without a barrier (91).

1 Mar 2005 20:17 AR AR246-MR35-05.tex XMLPublish^{SM}(2004/02/24) P1: JRX
AR REVIEWS IN ADVANCE10.1146/annurev.matsci.33.041002.094657

seeds were relatively large, it is likely that they all contained screw dislocations that could act as persistent step sources.

Whereas the habit plane of the twin in PMN/PT is incoherent, $BaTiO_3$ forms straight coherent twins on $\{111\}$ planes. When $BaTiO_3$ compacts are seeded with twinned grains, the twinned seeds outgrew the untwinned seeds, suggesting that a reentrant twin plane edge nucleation mechanism promotes abnormal growth (105). This is also suggested by observations of $BaTiO_3$ coarsened at temperatures in the range of 1350°C (where an intergranular liquid is expected to form), which showed that twinned grains grow larger than others (106). Rehrig et al. (25) independently measured the grain sizes of the large and small populations and showed that within experimental error, the sizes of the small grains had stopped increasing, whereas the large grains continued to increase in size. It should be noted that although the ideal version of the nucleation limited coarsening theory suggests that the growth of ideal (smaller) crystals should completely cease when they reach a size where the nucleation energy barrier becomes insurmountable (and this size should be in the nanometer size range), it does not account for finite volume fraction effects and growth from coalescence that is expected even in the absence of nucleation. In other words, there may be some growth by grain boundary migration, even in the absence of coarsening.

Finally, it should also be recognized that mechanisms for abnormal growth phenomena have also been proposed that have nothing to do with whether the interface is singular or rough. MacLaren et al. (107) observe AGG in alumina where the rapidly moving boundaries are clearly rough and have accumulated a disordered layer of impurities. They argue that at particular compositions, the impurities induce a structural transformation to a highly mobile boundary structure. It has also been demonstrated by simulation that grain boundaries with high mobility misorientations can be sustained if they grow into a highly textured matrix and that this can lead to abnormal growth (108). On the basis of these observations, it seems likely that a variety of possible explanations exist for abnormal growth in different systems. However, in systems that are sufficiently anisotropic, evidence pointing to the importance of the interface structure is accumulating.

CURRENT DIRECTIONS IN RESEARCH ON THE EFFECTS OF ANISOTROPY ON GROWTH

Now that it is possible to measure the anisotropy of the grain boundary character distribution, there are a number of questions that can be asked. First, does the grain boundary character distribution actually reach a statistically self-similar state, as indicated by simulation (77)? If so, in what way is it connected to the statistically self- similar grain size distribution? To answer these questions experimentally, the evolution of the distribution will have to be measured at different points in time. Assuming that a steady-state distribution does exist, it should be predictable by simulations using the grain boundary properties as input. It may also be possible

1 Mar 2005 20:17 AR AR246-MR35-05.tex XMLPublish^{SM}(2004/02/24) P1: JRX
AR REVIEWS IN ADVANCE10.1146/annurev.matsci.33.041002.094657

to develop an anisotropic theory for grain growth, in analogy to the classical grain growth theories, that allows the grain boundary character distribution to be predicted on the basis of anisotropic boundary properties. With such a theory, it might also be possible to work the inverse problem and determine the grain boundary properties from the experimentally observed grain boundary character distribution.

Assuming that the steady-state grain boundary character distribution is, in fact, a "fingerprint" of the microstructure, then it is sensible to ask how it is related to materials properties. If there is a direct correlation between certain materials properties and a predictable grain boundary character distribution, knowledge of this link should provide a path toward designing microstructures with predictable properties. In this case, it seems certain that research into the mechanisms of normal and abnormal growth phenomena will continue. The availability of three-dimensional anisotropic growth models will greatly aid this research because it will be possible to independently explore the influence of the grain boundary energy and mobility on the development of the grain boundary character distribution (77). It will also be possible to study the topology of the grain boundary network and the influence of initial orientation texture on the microstructures produced by growth. The recent emergence of new experimental tools will also advance this research by making it possible to collect the statistical data required to verify or refute hypothetical mechanisms for growth processes (69). For example, although abnormal growth remains a puzzle, with the proper data it should be possible to quantitatively assess the predictions of theories such as the one for nucleation limited coarsening described above.

ACKNOWLEDGMENT

This work was supported primarily by the MRSEC program of the National Science Foundation under Award Number DMR-00,79996 and partially by NASA under grant number 8-1674. I thank my colleagues at CMU who participated in this work, including W.W. Mullins, A.D. Rollett, D. Kinderlehrer, D. Saylor, T. Sano, C.-S. Kim, and J. Gruber. Helpful discussions with D.T. Wu and C.E. Krill, III, are also acknowledged.

LITERATURE CITED

1. Atkinson HV. 1988. Theories of normal grain growth in single phase systems. *Acta Metall.* 36:469–91
2. Fradkov VE, Udler D. 1994. Two-dimensional normal grain growth: topological aspects. *Adv. Phys.* 43:739–89
3. Voorhees PW. 1992. Ostwald ripening of two-phase mixtures. *Annu. Rev. Mater. Sci*. 22:197–215
4. Beck PA, Kremer JC, Demer L. 1947. Grain growth in high purity aluminum. *Phys. Rev.* 71:555

5. Beck PA, Holzworth ML, Hu H. 1948. Instantaneous rates of grain growth. *Phys. Rev.* 73:526–27
6. Burke JE. 1947. Grain growth in alpha-brass. *J. Appl. Phys.* 18:1028
7. Burke JE. 1949. Some factors affecting the rate of grain growth in metals. *Trans. Metall. Soc. AIME* 180:73–91
8. Lucke K, Detert K. 1957. A quantitative theory of grain boundary motion and recrystallization in metals in the presence of impurities. *Acta Metall.* 5:628–37
9. Cahn JW. 1962. The impurity-drag effect in grain boundary motion. *Acta Metall.* 10:789–98
10. Zener C. 1948. Grains, phases and interfaces: an interpretation of microstructure. *Trans. Metall. Soc. AIME* 175:15–51
11. Greenwood GW. 1956. The growth of dispersed precipitates in solutions. *Acta Metall*. 4:243–48
12. Grey EA, Higgins GT. 1973. Solute limited grain boundary migration: a rationalization of grain growth. *Acta Metall.* 21:309–21
13. Sun RC, Bauer CL. 1970. Measurements of grain boundary mobilities through magnification of capillary forces. *Acta Metall.* 18:635–48
14. Sun RC, Bauer CL. 1970. Tilt boundary migration in NaCl bicrystals. *Acta. Metall.* 18:639–47
15. Sun RC, Bauer CL. 1973. Kinetics of grain boundary migration in copper bicrystals with [001] rotation axes. *Acta Metall.* 21:1099–1109
16. Okazaki K, Conrad H. 1972. Grain size distribution in recrystallized alpha-titanium. *Trans. Jpn. Inst. Metals* 13:198–204
17. Hu H. 1974. Grain growth in zone refined iron. *Can. Metal. Q.* 13:275–86
18. Ardell AJ, Nicholson RB. 1966. The coarsening of gamma′ in Ni-Al Alloys. *J. Phys. Chem. Solids* 27:1793–804
19. Zhang C, Suzuki A, Ishimaru T, Enomoto M. 2004 Characterization of three-dimensional grain structure in polycrystalline iron by serial sectioning. *Metall. Mater. Trans.* 35A:1927–33
20. Döbrich KM, Rau C, Krill CE III. 2004. Quantitative characterization of the three-dimensional microstructure of polycrystalline Al-Sn using X-ray microtomography. *Metall. Mater. Trans* 35A:1953–61
21. Hull FC. 1988. Plane section and spatial characteristics of equiaxed β-brass grains. *Mater. Sci. Technol.* 4:778–85
22. Matsuura K, Itoh Y, Ohmi T, Ishii K. 1994. Evaluation of grain shape distribution in polycrystalline materials. *Mater. Trans. JIM* 35:247–53
23. Mahalingam K, Gu BP, Liedl GL, Sanders TH. 1987. Coarsening of delta (Al_3Li) precipitates in binary Al-Li alloys. *Acta Metall.* 35:483–98
24. Kim C-S. 2004. *Microstructural-mechanical property relationships in WC-Co composites*. PhD thesis. Carnegie Mellon Univ. 214 pp.
25. Rehrig PW, Messing GL, Trolier-McKinistry S. 2000. Templated grain growth of barium titanate single crystals. *J. Am. Ceram. Soc.* 83:2654–60
26. Smith CS. 1952. The shapes of metal grains, with some other metallurgical applications of topology. In *Metal Interfaces*, p. 65. Cleveland: ASM
27. Williams WM, Smith CS. 1952. A study of grain shape in an aluminum alloy and other applications of stereoscopic microradiaography. *J. Metals* 4:755–65
28. Marlow TR, Koch CC. 1996. Grain growth of nanocrystalline materials—a review. In *Synthesis and Processing of Nanocrystalline Materials*, ed. DL Bourell, pp. 33. Warrendale, PA: TMS
29. Gleiter H. 2000. Nanostructured materials: basic concepts and microstructure. *Acta Mater.* 48:1–29
30. Krill CE, Birringer R. 2001. Grain growth kinetics and thermal stability of nanoscrystalline materials. In *Recrystallization and Grain Growth*, ed. G Gottstein, DA Molodov, pp. 205–18. New York: Springer Verlag

31. Krill CE, Birringer R. 1998. Estimating grain-size distributions in nanocrystalline materials from X-ray diffraction profile analysis. *Philos. Mag. A* 77:621–40
32. Krill CE, Helfen RL, Michels D, Natter H, Fitch A, et al. 2001. Size-dependent grain-growth kinetics observed in nanocrystalline Fe. *Phys. Rev. Lett.* 86:842–45
33. Weissmuller J. 1994. Alloy thermodynamics in nanostructures. *J. Mater. Res.* 9:4–7
34. Krill CE, Klein R, Janus S, Birringer R. 1995. Thermodynamic stabilization of grain boundaries in nanocrystalline alloys. *Mater Sci. Forum* 179–181:443–48
35. Lifshitz IM, Slyozov VV. 1961. The kinetics of precipitation from saturated solids solutions. *J. Phys. Chem. Solids* 19:35–50
36. Wagner C. 1961. Theorie der Alterung Niederschlagen durch Umlosen. *Z. Elektrochem.* 65:581–91
37. Ardell AJ. 1972. The effect of volume fraction on particle coarsening: theoretical considerations. *Acta Metall.* 20:61–71
38. Davies CKL, Nash P, Stevens RN. 1980. The effect of volume fraction of precipitate on Ostwald ripening. *Acta Metall.* 28:179–89
39. Voorhees PW, Glicksman ME. 1984. Solution to the multi-particle diffusion problem with applications to Ostwald ripening—I. Theory. *Acta Metall.* 32:2001–11
40. Mullins WW. 1956. Two dimensional motion of idealized grain boundaries. *J. Appl. Phys.* 27:900–4
41. Mullins WW. 1989. Estimation of the geometrical rate constant in idealized three dimensional grain growth. *Acta Metall.* 37:2979–84
42. Hilgenfeldt S, Kraynik AM, Koehler SA, Stone HA. 2001. An accurate von Neumann's law for three-dimensional foams. *Phys. Rev. Lett.* 86:2685–99
43. Deleted in proof
44. Deleted in proof
45. Glicksman M. 2004. Capillarity-mediated grain growth in 3-D. *Mater Sci. Forum* 467–470:1025–32
46. Hillert M. 1965. On the theory of normal and abnormal grain growth. *Acta Metall.* 13:227–38
47. Louat NP. 1974. On the theory of normal grain growth. *Acta Metall.* 22:721–24
48. Pande CS. 1987. On a statistical theory of grain growth. *Acta Metall.* 35:2671–78
49. Ryum N, Hunderi O. 1989. On the analytic description of normal grain growth. *Acta Metall.* 37:1375–79
50. Thorvaldson A. 1993. Grain growth as a stochastic process. *Acta Metall. Mater.* 41:1347–57
51. Mulheran PA. 1992. Mean field simulations of normal grain growth. *Acta Metall. Mater.* 40:1827–33

51a. Wu DT. 1994. Mass conservation in grain growth. *Mater. Res. Symp. Proc.* 343:61–64

52. Mullins WW. 1998. *Models of idealized grain growth: critique of stochastic theories and implications of scaling*. Presented at Proc. Int. Conf. Grain Growth, Pittsburgh, PA, p. 353
53. Mullins WW. 1998. Grain growth of uniform boundaries with scaling. *Acta Mater*. 46:6219–26
54. Anderson MP, Grest GS, Srolovitz DJ. 1989. Computer simulation of normal grain growth in three dimensions. *Philos. Mag. B* 59:293–329
55. Fuchizaki K, Kusaba T, Kawasaki K. 1995. Computer modelling of three-dimensional cellular pattern growth. *Philos. Mag. B* 71:333–57
56. Wegand D, Brechet Y, Lepinoux J, Gust W. 1999. Three-dimensional grain growth: a vertex dynamics simulation. *Philos. Mag. B* 79:703–16
57. Wakai F, Enomoto N, Ogawa H. 2000. Three-dimensional microstructural evolution in ideal grain growth-general statistics. *Acta Mater.* 48:1297–311
58. Krill CE, Chen L-Q. 2002. Computer simulation of 3-D grain growth using a phase field model. *Acta Mater.* 50:3057–73

1 Mar 2005 20:17 AR AR246-MR35-05.tex XMLPublish^{SM}(2004/02/24) P1: JRX
AR REVIEWS IN ADVANCE10.1146/annurev.matsci.33.041002.094657

59. Kuprat AP. 2000. Modeling microstructure evolution using gradient-weighted moving finite elements. *SIAM J. Sci. Comput.* 22:535–60
60. Gottstein G, King AH, Shvindlerman LS. 2000. The effect of triple-junction drag on grain growth. *Acta Mater.* 48:397–403
61. Estrin Y, Gottstein G, Shvindlerman LS. 1999. Intermittent 'self-locking' of grain growth in fine-grained materials. *Scripta Mater.* 41:385–90
62. Estrin Y, Gottstein G, Rabkin E, Shvindlerman LS. 2000. On the kinetics of grain growth inhibited by vacancy generation. *Scripta Mater.* 43:141–47
63. Adams BL, Kinderlehrer K, Livshits I, Mason DE, Mullins WW, et al. 1999. extracting grain boundary and surface energy from measurement of triple junction geometry. *Interface Sci.* 7:321
64. Helfen L, Wu DT, Birringer R, Krill CE. 2003. The impact of stochastic atomic jumps on the kinetics of curvature-driven grain growth. *Acta Mater.* 51:2743–54
65. Saylor DM, Mason DE, Rohrer GS. 2000. Experimental method for determining surface energy anisotropy and its application to magnesia. *J. Am. Ceram. Soc.* 83:1226–32
66. Kitayama K, Glaeser AM. 2002. The Wulff shape of alumina: III, undoped alumina. *J. Am. Ceram. Soc.* 85:611–22
67. Hasson GC, Goux C. 1971. Interfacial energies of tilt boundaries in aluminum. Experimental and theoretical determination. *Scripta Metall.* 5:889–94
68. Gottstein G, Shvindlerman LS. 1999. *Grain Boundary Migration in Metals*. Boca Raton, FLL CRC Press
69. Rohrer GS, Saylor DM, El-Dasher BS, Adams BL, Rollett AD, Wynblatt P. 2004. The distribution of internal interfaces in polycrystals. *Z. Metall.* 95:197–214
70. Saylor DM, Morawiec A, Rohrer GS. 2003. Distribution of grain boundaries in magnesia as a function of five macroscopic parameters. *Acta Mater.* 51:3663–74
71. Saylor DM, El-Dasher BS, Sano T, Rohrer GS. 2004. Distribution of grain boundaries in $SrTiO_3$ as a function of five macroscopic parameters. *J. Am. Ceram. Soc.* 87:670–76
72. Saylor DM, El-Dasher BS, Pang Y, Miller HM, Wynblatt P, et al. 2004. Habits of grains in dense polycrystalline solids. *J. Am. Ceram. Soc.* 87:724–26
73. Miller HM, Saylor DM, El-Dasher BS, Rollett AD, Rohrer GS. 2004. Crystallographic distribution of internal interfaces in spinel polycrystals. *Mater Sci. Forum* 467–470:783–88
74. Saylor DM, El-Dasher BS, Rollett AD, Rohrer GS. 2004. Distribution of grain boundaries in aluminum as a function of five macroscopic parameters. *Acta Mater.* 52:3649–55
75. Bennett TA, Kim C-S, Rohrer GS, Rollett AD. 2004. Five-parameter grain boundary character distribution in Fe-1%Si. *Mater Sci. Forum* 467–470:1057–62
76. Saylor DM, Morawiec A, Rohrer GS. 2003. The relative free energies of grain boundaries in magnesia as a function of five macroscopic parameters. *Acta Mater.* 51:3675–86
77. Gruber J, George DC, Kuprat AP, Rohrer GS, Rollett AD. 2004. Effect of anisotropic interfacial energy on grain boundary distributions during grain growth. *Mater Sci. Forum* 467–470:733–38
78. Demirel MC, Kuprat AP, George DC, Rollett AD. 2003. Bridging simulations and experiments in microstructure evolution. *Phys. Rev. Lett.* 90:016106
79. Mullins WW. 1986. The statistical self similarity hypothesis in grain growth and particle coarsening. *J. Appl. Phys.* 59: 1341–49
80. Mullins WW, Vinals J. 1993. Scaling in linear bubble models of grain growth. *Acta Mater.* 41:1359–67

81. Rutenberg AD, Vollmayr-Lee BP. 1999. Anisotropic coarsening: grain shapes and nonuniversal persistence. *Phys. Rev. Lett.* 83:3772–75
82. Brosh E, Shneck RZ. 2000. Anisotropic coarsening: the effect of interfacial properties on the shape of grains. *Model. Simul. Mater. Sci. Eng.* 8:815–23
83. Sano T, Kim C-S, Rohrer GS. 2005. Shape evolution of $SrTiO_3$ crystals during coarsening in a titania-rich liquid. *J. Am. Ceram. Soc*. In press
84. Gorzkowski EP, Chan HM, Harmer MP, Sano T, Kim C-S, Rohrer GS. 2005. Changes in the distribution of interfaces in PMN-35 mol% PT as a function of time. *Z. Metall*. In press
85. Holm EA, Hassold GN, Miodownik MA. 2001. On misorientation distribution evolution during anisotropic grain growth. *Acta Mater.* 49:2981–91
86. Upmanyu U, Hassold GN, Kazaryan A, Holm EA, Wang Y, et al. 2002. Boundary mobility and energy anisotropy effects on microstructural evolution during grain growth. *Interface Sci.* 10:201–16
87. Kinderlehrer D, Livshits I, Rohrer GS, Ta'asan S, Yu P. 2004. Mesoscale simulation of the evolution of the grain boundary character distribution. *Mater Sci. Forum* 467–470:1063–68
88. Rollett AD. 2004. Crystallographic texture changes during grain growth. *J. Met.* 56:63–68
89. Yang C-C, Rollett AD, Mullins WW. 2001. Measuring relative grain boundary energies and mobilities in an aluminum foil from triple junction geometry. *Scripta Met.* 44:2735–40
90. Burton WK, Cabrera N, Frank FC. 1951. The growth of crystals and the equilibrium structure of their surfaces. *Philos. Trans. R. Soc. London Ser. A* 243:300–58
91. Rohrer GS, Rohrer CL, Mullins WW. 2002. Coarsening of faceted crystals. *J. Am. Ceram. Soc.* 85:675–82
92. Mullins WW, Rohrer GS. 2000. Nucleation barrier for volume conserving shape changes of faceted crystals. *J. Am. Ceram. Soc.* 83:214–16
93. Sheldon BW, Rankin J. 2002. Step-energy barriers and particle shape changes during coarsening. *J. Am. Ceram. Soc.* 85:683–90
94. Weeks JD, Gilmer GH. 1979. Dynamics of crystal growth. *Adv. Chem. Phys*. 40:157–228
95. Peteves SD, Abbaschian R. 1991. Growth kinetics of solid-liquid Ga interfaces: Part I. Experimental. *Metall. Mater. Trans.* 22A:1259–70
96. Peteves SD, Abbaschian R. 1991. Growth kinetics of solid-liquid Ga interfaces: Part II. Theoretical. *Metall. Mater. Trans.* 22A:1271–86
97. Keller KW. 1986. Modes of crystal growth revealed by electron microscopy on NaCl. *J. Cryst. Growth* 74:161–71
98. Yoon D-Y, Cho YK. 2005. Roughening transition of grain boundaries in metals and oxides. *Interface Sci.* In press
99. Oh K-S, Jun J-Y, Kim D-Y, Hwang N-M. 2000. Shape dependence of the coarsening behavior of niobium carbide grains dispersed in a liquid iron matrix. *J. Am. Ceram. Soc.* 83:3117–20
100. Chung S-Y Kang S-JL. 2000. Effect of dislocations on grain growth in $SrTiO_3$. *J. Am. Ceram. Soc.* 83:2828–32
101. Wallace JS, Huh J-M, Blendell JE, Handwerker CA. 2002. Grain growth and twin formation in 0.74PMN·0.26PT. *J. Am. Ceram. Soc.* 85:1581–84
102. Chung U-J, Park J-K, Hwang N-M, Lee H-Y, Kim D-Y. 2002. Effect of grain coalescence on the abnormal grain growth of $Pb(Mg_{1/3}Nb_{2/3})O_3$ 35 mol% $PbTiO_3$ ceramics. *J. Am. Ceram. Soc.* 85:965–68
103. Warrington DH, Boon M. Ordered structures in random grain boundaries; some geometrical probabilities. *Acta Metall.* 23:599–607
104. Rockosi DJ, Gorzkowski EP, King PT, Scotch AM, Chan HM, Harmer MP. 2004. Seeded growth from twinned

1 Mar 2005 20:17 AR AR246-MR35-05.tex XMLPublish^{SM}(2004/02/24) P1: JRX
AR REVIEWS IN ADVANCE10.1146/annurev.matsci.33.041002.094657

and untwinned abnormal grains of Pb $(Mg_{1/3}Nb_{2/3})O_3$ 35 mol% $PbTiO_3$ in a matrix containing PbO additions. *J. Am. Ceram. Soc.* 87:1339–42

105. Kang M-K, Yoo Y-S, Kim D-Y, Hwang N-M. 2000. Growth of $BaTiO_3$ seed grains by the twin-plane reentrant edge mechanism. *J. Am. Ceram. Soc.* 83:385–90
106. Lee H-Y, Kim J-S, Kim D-Y. 2002. Effect of twin plane reentrant edge on the coarsening behavior of barium titanate grains. *J. Am. Ceram. Soc.* 85:977–80
107. Maclaren I, Cannon RM, Gulgun MA, Voytovych R, Popescu-Pogrion N, et al. 2003. Abnormal grain growth in alumina: synergistic effects of yttria and silica. *J. Am. Ceram. Soc.* 86:650–59
108. Holm EA, Miodownik MS, Rollett AD. 2003. On abnormal subgrain growth and the origin of recrystallization nuclei. *Acta Mater.* 51:2701–16